

# FEM modeling and comparative study of graphite lubricants in the hot forging of AISI 1045 medium carbon steel

Raschanan POUNGPRASERT<sup>1</sup>, Nattarawee SIRIPATH<sup>1</sup>, Naiyanut JANTEPA<sup>1</sup>, and Surasak SURANUNTCHAI<sup>1,\*</sup>

<sup>1</sup> King Mongkut's University of Technology Thonburi, Pracha Uthit Rd, Bang Mot, Thung Khru, 10140, Bangkok

#### Received date:

20 February 2025

Revised date:

17 July 2025

#### Accepted date:

8 September 2025

#### **Keywords:**

Lubricant; Friction factor; Hot forging; Ball joint; FEM

#### Abstract

This study investigates the performance of water-based and oil-based graphite lubricants in the hot forging of AISI 1045 medium carbon steel, aiming to enhance product quality while minimizing die wear. Utilizing Finite Element Method (FEM) simulations and experimental analysis, we examined key factors including flow lines, dimensional accuracy, forging load, and die wear. Results indicate that oil-based graphite lubricants significantly outperform water-based options, achieving a lower average error of 0.26% in dimensional accuracy compared to 0.99% for water-based lubricants. Additionally, oil-based lubricants resulted in reduced forming loads, leading to improved energy efficiency and longer die life. Microstructural analysis revealed that oil-based lubrication yielded an average grain size of 13.50 μm, 42.60% finer than the 23.52 μm observed with water-based lubricants, enhancing mechanical properties due to the Hall-Petch relationship. Furthermore, FEM simulations demonstrated that oil-based lubricants produced lower stress levels in dies, correlating with reduced wear. Overall, the findings suggest that oil-based graphite lubricants provide superior performance in hot forging applications, enhancing manufacturing efficiency and product quality. This research underscores the importance of lubricant selection in optimizing forging processes for improved cost-effectiveness and durability in production.

#### 1. Introduction

Hot forming is a pivotal technique in metal shaping that involves heating metals to high temperatures, allowing for recrystallization without reaching their melting points. This method is particularly suitable for producing complex components in large quantities, making it a crucial process in various industries, including automotive, aerospace, agriculture, and construction. Among the various hot forming techniques, hot forging stands out as a widely utilized method that applies pressure to a die to create desired shapes, resulting in products renowned for their exceptional strength and durability [1].

Despite its advantages, a significant challenge in achieving highquality results in hot forging is managing the friction between the flow, introduce defects, and lead to non-uniform shapes, ultimately die and the workpiece [2]. Excessive friction can disrupt material compromising the integrity of the final product [3,4]. Therefore, effective lubrication is crucial for minimizing friction and ensuring consistent, defect-free components. High friction not only increases the required forging force—leading to higher energy consumption but also accelerates die wear, resulting in increased operational costs and potential dimensional inconsistencies. Furthermore, the heat generated from friction can alter material properties and adversely affect surface finish, jeopardizing product accuracy [5,6].

To achieve effective control over friction, it is essential to conduct a comprehensive investigation of lubrication's impact. The lubrication systems typically employed for hot forging carbon steel often incorporate graphite in an aqueous solution [7]. Numerous studies have sought to understand the influence of friction and wear in hot forging processes, specifically examining the role of lubricants in reducing tool wear and improving product quality. For instance, Barrau et al. [8] highlighted the critical relationship between friction and energy consumption during forging, demonstrating that tool life is often limited by wear mechanisms such as abrasion, plastic deformation, and thermal fatigue. Their research on AISI H11 steel revealed that wear behavior is highly temperature-dependent, with friction significantly decreasing at temperatures above 800°C. Building on this foundation, further research has explored the role of lubricants in detail. Daouben et al. [9] conducted friction tests under hot forging conditions using graphitebased lubricants and found that lubricant film thickness and particle size are key factors influencing wear in the flash zone of nitrided steel dies. Similarly, Zhu et al. [10] emphasized the importance of accurately determining the heat transfer coefficient (HT) when evaluating friction in hot forging, as variations in HT significantly impact metal flow and interfacial friction. Asai and Kitamura [11,12] extended these studies by evaluating the tribological performance of both graphite and non-graphite lubricants in hot forging, finding that non-graphite

<sup>\*</sup>Corresponding author e-mail: surasak.sur@kmutt.ac.th

lubricants were inadequate at temperatures exceeding 450°C. Their finite element modeling (FEM) analysis improved the precision of friction coefficient measurements by updating calibration curves to incorporate heat transfer and contact velocity. More recently, Serebriakov et al. [13] investigated interfacial friction during hot forging in the railway industry, highlighting how oxide particles influence lubricant breakdown and alter interfacial conditions. Collectively, these studies provide valuable insights into the role of graphite lubricants in mitigating wear and optimizing friction during the hot forging of medium carbon steels like AISI 1045.

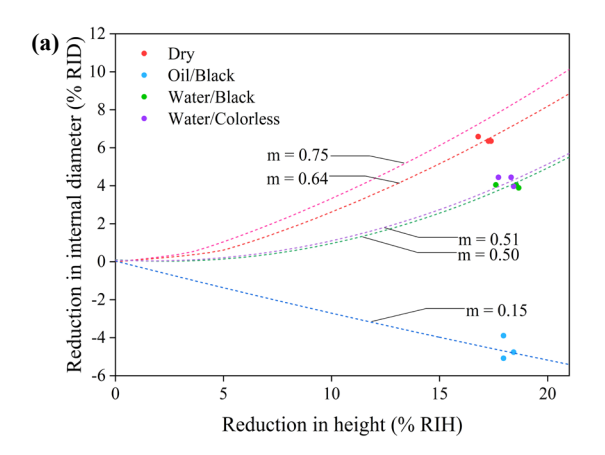
To address these challenges effectively, the selection of efficient lubricants is paramount. They not only enhance product quality and extend tool life by reducing forging load and wear but also prevent direct metallic contact between the tool and workpiece. However, if a lubricant fails to withstand the harsh conditions of hot forging, it can lead to product defects or tool failure. Moreover, the physical and chemical properties of the materials at the tool-billet interface play a significant role in influencing wear and surface quality, which further impacts the forging outcome. One of the most reliable tribological tests for evaluating friction in bulk and sheet metal forming is the ring compression test, where a ring-shaped specimen undergoes uniaxial plastic compression between flat platens [14,15]. The change in the inner diameter during this process is contingent on the friction at the ring-platens interface, necessitating precise calibration through experimental measurements and numerical simulations. Previous research has explored the impact of lubrication on friction in hot forging processes, particularly for AISI 1045 medium carbon steel using ring compression tests [14,15]. Poungprasert et al. [16] developed predictive calibration curves (Figure 1(a)) through FEM to enhance friction factor estimations by monitoring dimensional changes during compression. Their analysis of various lubrication conditions—including dry, oil with black graphite, water with black graphite, and water with colorless graphite—demonstrated that lubrication significantly reduces friction, with oil containing black graphite showing the best performance. These findings are critical for optimizing lubricant selection and improving the accuracy of hot forging simulations. It is important to note that while this study focuses on BS 080M46, this material is equivalent to AISI 1045 in terms of chemical composition and mechanical properties, differing only in standard designation. Thus, the results can be applied to both BS 080M46 and AISI 1045, broadening the relevance of these findings to international applications in medium carbon steel hot forging processes. In further studies, Srivastava et al. [17] aimed to determine the friction factor and coefficient of friction by compressing a standard-sized aluminum alloy ring under various conditions, revealing that the load required to deform the specimen remained largely insensitive to friction conditions. In contrast, Lima and Button [18] underscored the importance of computational modeling in cold forging processes, utilizing ANSYS to simulate forming operations and validate experimental data for enhanced design efficiency. Furthermore, Shahriari et al. [19], examined the influence of temperature and lubricant type on friction coefficients in the hot forging of Nimonic 115, employing ring compression tests and 3D finite element simulations to recommend mica as an effective lubricant, achieving a friction coefficient of approximately 0.3. Collectively, these studies underscore the critical role of friction in metal forming processes and emphasize the need for precise measurement and modeling techniques to enhance manufacturing efficiency.

This study aims to compare water-based and oil-based graphite lubricants in the hot forging of AISI 1045 medium carbon steel, focusing on their effectiveness in reducing friction and improving product quality. By employing FEM simulations and experimental methods, the research investigates various factors, including flow lines, defects, dimensional accuracy, temperature distribution, surface finish, and forging load. Additionally, it evaluates die wear, a crucial factor in the longevity and maintenance of forging equipment. Ultimately, the goal is to determine which lubricant enhances manufacturing efficiency and the quality of forged ball joints while minimizing die wear, leading to more cost-effective and durable production processes.

## 2. Methodology

#### 2.1 Materials

In this current work, AISI 1045 medium carbon steel was investigated. The chemical composition (in weight percentages) was determined using an emission spectrometer on two test specimens, yielding the following results: C 0.4671%, Mn 0.673%, Si 0.1940%, Cu 0.1780%, Ni 0.0682%, P 0.0265%, S 0.0214%, Mo 0.0155%, with Fe constituting the balance. These values align well with the standard composition of AISI 1045 steel, as shown in Table 1.



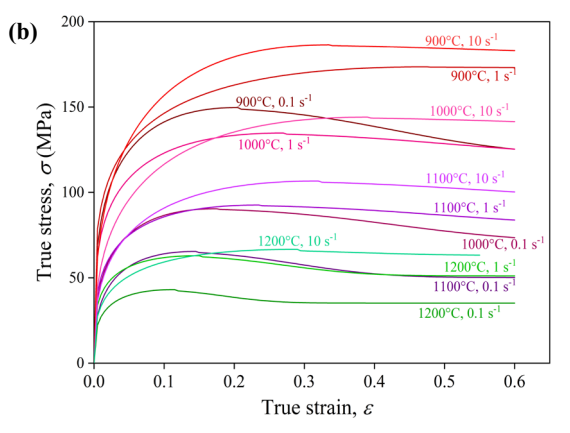


**Figure 1**. (a) Predictive calibration curve and experimental results at different lubricant, sourced from Poungprasert, *et al.* [16], and (b) True stress—True strain from the hot compression test at strain rates of  $0.1 \text{ s}^{-1}$ ,  $1 \text{ s}^{-1}$ , and  $10 \text{ s}^{-1}$  under various deformation conditions.

Table 1. Chemical composition of AISI 1045 steel according to the AISI standard [20].

C	Mn	P	S
0.43-0.50	0.60-0.90	0.04Max.	0.05Max.

**Table 2.** Mechanical crank press machine specification.

Classification	Capacity	Stroke	Stroke per mir	n Die height	Slide adjust	Bed area	Slide area	Main motoe
	[ton]	[mm]		[mm]	[mm]	[mm]	[mm]	[kW]
JFP-1350	1350	240	85	720	8	1030 × 1060	880 × 920	75

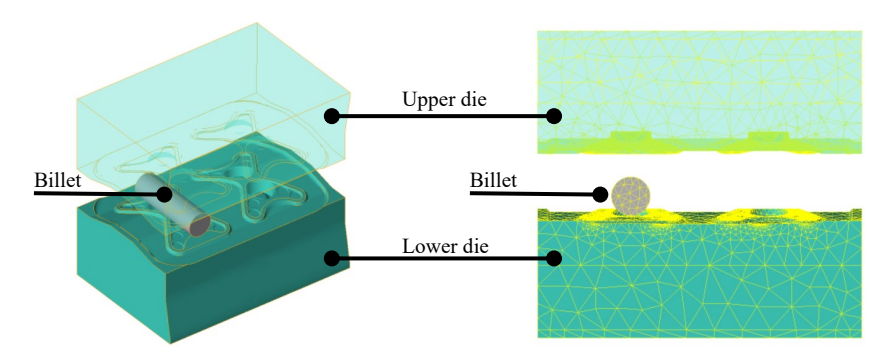


Figure 2. 3D-FEM of the Hot Forging Process for Ball Joint Manufacturing.

Cylindrical samples with a diameter of 5 mm and a height of 10 mm were prepared for hot compression tests. These tests were conducted using a Baehr DIL-805 deformation dilatometer, with the testing temperature measured directly by a thermocouple. The hot compression tests were carried out at temperatures of 900°C, 1000°C, 1100°C, and 1200°C, and at strain rates of 0.1 s<sup>-1</sup>, 1 s<sup>-1</sup>, and 10 s<sup>-1</sup>, all within a vacuum chamber filled with argon gas. The samples were heated to the test temperatures at a rate of 1.625°C·s<sup>-1</sup> using an induction coil, held at the target temperature for 1 min, and then compressed to a 60% height reduction using an alumina punch. After compression, the samples were quenched in argon gas at a rate of 40°C·s<sup>-1</sup> until they reached room temperature. Figure 1(b) shows the true stress-true strain curves at various deformation conditions.

The validation of FEM simulation results was conducted through detailed grain size. Cut samples were hot-mounted to ensure stability, then polished sequentially using 400 grit, 600 grit, 800 grit, 1000 grit, and 1200-grit SiC papers. Final polishing was performed with a 0.3  $\mu$ m alumina suspension to achieve a mirror-like surface suitable for microstructural observation.

The polished samples were etched for 4 s in both 4% picral and 3% Nital solutions to reveal grain boundaries and phase distribution. Microstructural examination was conducted using light optical microscopy (LOM), focusing on the central region of the cross-sections to capture representative deformation features. Grain size was determined following the metallographic method as per ASTM E1382, providing accurate and consistent measurements for validating FEM simulation results.

## 2.2 Hot forging process of ball joint

The ball joint was manufactured through a hot forging process using AISI 1045 medium carbon steel. The tooling set, consisting of upper and lower dies made from SKD61 steel, was preheated to 250°C. The forging process began by heating the billet in a furnace

to 1100°C, followed by two stages in a mechanical press: roughing and finishing. After the final forging step, the flash was removed, and the workpiece was left to cool to ambient temperature. A graphite-based lubricant was applied to the working surfaces during both the roughing and finishing stages to ensure smooth operation. This lubricant reduced friction, cooled the tools, prevented sticking and galling, and minimized wear on the die surfaces. Further details on the lubricant can be found in Section 2.2. The forging process was performed using a 1350-ton mechanical crank press, whose specifications are listed in Table 2.

#### 2.3 Lubricant

Two different types of graphite-based lubricants were studied: black graphite mixed with water and black graphite mixed with oil in a 1:20 ratio. The characteristics of these lubricants are summarized as follows: The graphite-to-water lubricant, labeled RAMUDO MF161, has a density of 1.1 g·cm<sup>-3</sup>, a pH of approximately 11, and a viscosity of around 800 Cp at 25°C. The graphite-to-oil lubricant, labeled RAMUDO L120, does not have a specified density or viscosity, but its pH ranges from 6.5 to 9.5. These details are referenced from the product datasheet [21-24].

#### 2.4 FE simulation of ball joint

FEM simulation models for the hot forging process of a ball joint made from AISI 1045 medium carbon steel were developed using QForm V10.1.6 commercial software. The assembly CAD file, provided by S.B.-CERA Co., Ltd., was imported into QForm V10.1.6. The 3D CAD model includes the upper die, lower die, and billet. Tetrahedral elements were generated for the Finite Element (FE) model, as illustrated in Figure 2. The cylindrical billet was set as plastic, and the tooling as rigid. The simulation conditions were based on the actual hot forging

process used for the ball joint. Ambient conditions such as temperature and cooling rates were set according to values provided by the software's built-in library. For the bulk deformation process, shear-type friction was assumed to account for the material's shear deformation behavior. Friction coefficients were specified as follows: 0.15 for oil-based lubrication with black graphite and 0.5 for water-based lubrication with black graphite. These values were referenced from previous research [16], ensuring accurate representation of lubrication effects during the forging process.

#### 3. Results and discussion

#### 3.1 Modeling the constitutive equation

A constitutive equation is essential for describing the stress-strain behavior of materials. By using experimentally derived true stress-strain curves from hot deformation, material constants can be precisely determined through a well-established constitutive model [25]. One widely recognized approach to characterize this behavior is with the Zener-Hollomon parameter (Z), which expresses the relationship between strain rate ( $\dot{\varepsilon}$ ) and temperature (T) during plastic deformation [26-28], as illustrated in Equation (1). Sellars and McTegart introduced the Arrhenius-type constitutive model (Equation (2)), which effectively captures the relationship between flow stress, strain rate, and deformation temperature [29,30].

$$Z = \dot{\varepsilon} \exp(Q/RT) \tag{1}$$

$$\dot{\varepsilon} = Z \exp(-Q/RT) = F(\sigma) \exp(-Q/RT)$$
 (2)

In these equations,  $F(\sigma)$  represents the stress function, which varies depending on the deformation conditions which can be described by Equation (3). Q denotes the activation energy for deformation (kJ·mol<sup>-1</sup>), a material-specific property, while R is the universal gas constant (8.314 J·mol<sup>-1</sup>·K), T is the absolute temperature in Kelvin, and  $\sigma$  represents the applied stress on the material (MPa).

$$F(\sigma) = Z = \begin{cases} A_1 \sigma^m &: \alpha \sigma < 0.8 \\ A_2 \exp(\beta \sigma) &: \alpha \sigma > 1.2 \\ A_3 \left[ \sinh(\alpha \sigma) \right]^n : \text{ for all } \sigma \end{cases}$$
(3)

where  $A_1$ ,  $A_2$ ,  $A_3$ , m, n,  $\alpha$  and  $\beta$  are material constants. The material constants for the Zener-Hollomon equation are derived based on relations from peak stress values [31,32]. Specifically, m and  $\beta$  are obtained by substituting the power-law and exponential forms of Equation (3) into Equation (2) at lower stress levels ( $\alpha\sigma < 0.8$ ) and higher stress levels ( $\alpha\sigma > 1.2$ ), respectively. Taking the natural logarithm of both sides of each equation then leads to the following expressions:

$$\ln \dot{\varepsilon} = m \ln \sigma + \ln A_1 - Q/RT \tag{4}$$

$$\ln \dot{\varepsilon} = \beta \sigma + \ln A_2 - (Q/RT) \tag{5}$$

Considering that the hot deformation was performed at a constant temperature, partial differentiation of Equation (4) and Equation (5), respectively, yields Equation (6) and Equation (7):

$$m = \left[ \frac{\partial \ln \dot{\varepsilon}}{\partial \ln \sigma} \right]_T \tag{6}$$

$$\beta = \left[ \frac{\partial \ln \dot{\varepsilon}}{\partial \sigma} \right]_{T} \tag{7}$$

The material constants are determined using the linear regression method. The values of m and  $\beta$  are obtained from the average slopes of the individual fitted lines in the plots of  $\ln \dot{\varepsilon} - \ln \sigma$  and  $\ln \dot{\varepsilon} - \sigma$ , as shown in Figure 3(a-b). The activation energy Q is then calculated by substituting the hyperbolic sine law of Equation (3) into Equation (2) for all range of stress levels. Applying the natural logarithm to both sides of each equation in Equation (8).

$$\ln \dot{\varepsilon} = \ln A + n \ln[\sinh(\alpha \sigma_{p})] - (Q/RT)$$
 (8)

Through partial differentiation of Equation (8), the apparent activation energy Q can be expressed as follows:

$$Q = R \left[ \frac{\partial \ln(\dot{\varepsilon})}{\partial \ln[\sinh(\alpha\sigma)]} \right]_{T} \left[ \frac{\partial \ln[\sinh(\alpha\sigma)]}{\partial (1/T)} \right]_{L}$$
(9)

According to Equation (5), Q is calculated from the slopes observed in the scatter plots of  $\ln \dot{\varepsilon} - \ln[\sinh(\alpha\sigma)]$  for constant temperature and  $\frac{1}{T} - \ln[\sinh(\alpha\sigma)]$  for constant strain rate, as shown in Figure 3c-d), respectively. The value of Q can be determined by averaging the values obtained at different strain rates and deformation temperatures. By employing Equation (1-3), as depicted in Equation (10), allows for the establishment of a relationship between the Z parameter and true stress. Moreover, applying the natural logarithm to both sides of each Equation (10) leads to a modified equation represented as Equation (11):

$$Z = \dot{\varepsilon} \exp(Q/RT) = A[\sinh(\alpha\sigma)]^{n}$$
 (10)

$$\ln Z = \ln A + n \ln \left[ \sinh(\alpha \sigma) \right] \tag{11}$$

The scatter plot of  $\ln Z - \ln[\sinh(\alpha\sigma)]$  shown in Figure 3(e) demonstrates a strong linear correlation, suggesting a good fit. The intercept and slope of this plot represent the values of A and n, respectively. The material constants for the Arrhenius-based constitutive model of AISI 1045 medium carbon steel are presented in Table 3.

Based on Equation (10), it is possible to express the flow stress of the material at a specific strain as a function of the Zener-Hollomon parameter, considering the definition of the hyperbolic sine law. The following expression can be derived:

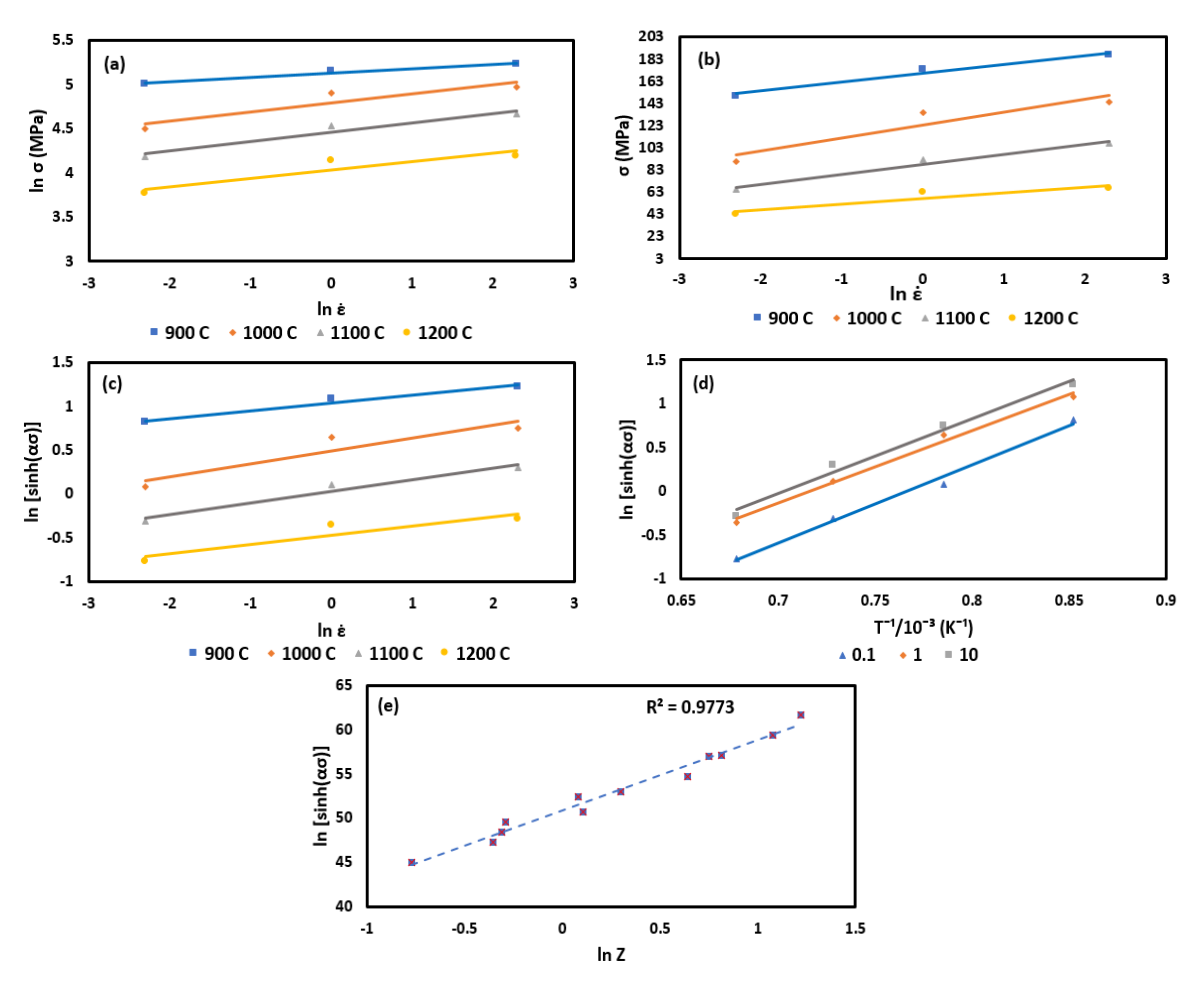


**Figure 3**. Plots illustrating the relationship between (a)  $\sigma$ -  $\ln \dot{\varepsilon}$ ; (b)  $\ln \sigma$ -  $\ln \dot{\varepsilon}$ ; (c)  $\ln \left[\sinh(\alpha \sigma)\right] - \ln \dot{\varepsilon}$ ; (d)  $\ln \left[\sinh(\alpha \sigma)\right] - 1000/T$ ; and (e)  $\ln \left[\sinh(\alpha \sigma)\right] - \ln Z$ .

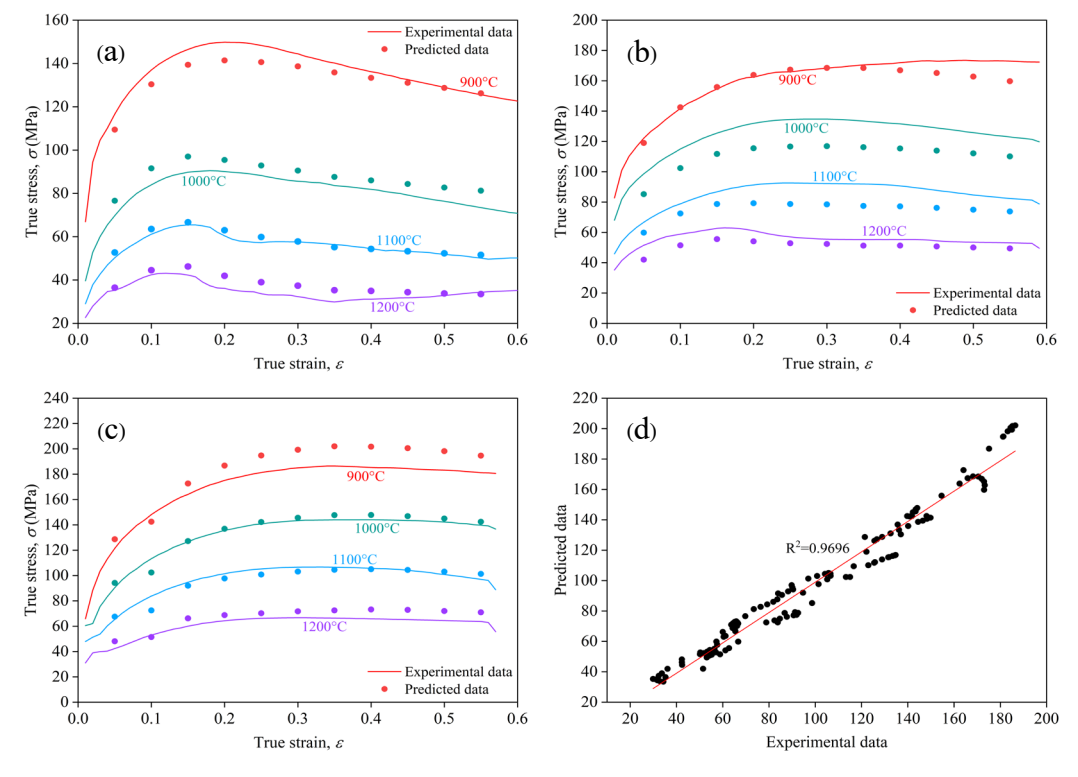


**Figure 4**. Comparing the experimental flow curves with prediction from Arrhenius-based Constitutive equation of AISI 1045 medium carbon steel under various deformation conditions..

Table 3 Material constants for the general expression of the Arrhenius-based constitutive model, derived from peak stress values.

m	β	α	n	Q	$\ln A$	A
11.4600	0.1185	0.01037	8.0914	578.9597	50.8455	$1.2076 \times 10^{22}$

Table 4 Comparison of thickness (mm) at different sections of the actual forged product formed using water-based and oil-based graphite lubricants.

Section	Spec	Oil-based graphite					Water-based graphite				
		1	2	3	Mean	Error	1	2	3	Mean	Error
A	43.00	42.80	42.95	42.85	42.86	0.32%	42.90	43.05	43.15	43.03	0.07%
В	10.50	10.45	10.50	10.50	10.43	0.67%	10.90	10.75	10.70	10.85	3.33%
C	47.8	47.80	47.80	47.80	47.80	0.00%	47.55	47.55	47.85	47.65	0.31%
D	49.4	49.30	49.40	49.30	49.33	0.06%	49.10	49.30	49.40	49.27	0.26%
Average						0.26%					0.99%

$$\sigma = \frac{1}{\alpha} \sinh^{-1} \left( \frac{Z}{A} \right)^{\frac{1}{n}} \tag{12}$$

$$\sigma = \frac{1}{\alpha} \sinh^{-1} \left( \frac{1}{A} \cdot \dot{\varepsilon} \cdot \exp\left(\frac{Q}{RT}\right) \right)^{\frac{1}{n}}$$
 (13)

To generate the predicted flow curve, the relevant material constants in Table 3 for each deformation condition are substituted into these equations. The predicted flow curve is then compared with experimental data, as shown in Figure 4. The flow stresses predicted by the constitutive models closely match the experimental data, demonstrating their reliability and precision at high temperatures. To evaluate this accuracy, three statistical parameters were employed: the average absolute relative error (AARE), root mean square (RMS), and correlation coefficient (R²) [33,34]. The results indicate a high level of accuracy in the prediction model, with an R² value of 0.9696 and an AARE of 6.824% (Figure 4(d)). Furthermore, the constitutive models based on the Arrhenius equation were implemented into finite element software to optimize the manufacturing process conditions for the ball joint.

## 3.2 Accuracy of the forged product

The ball joint, a key component in automotive applications, was manufactured using a two-step forging process: roughing and finishing. The roughing stage served to distribute material mass and prepare the workpiece for the subsequent finishing stage, in which the final shape and dimensions were achieved. After forging, a flash trimming operation was carried out to remove excess material. The final shape of the ball joint is illustrated in Figure 5(a). A commendable level of precision was observed in the thickness measurements across four different sections of the forged product, formed using both waterbased and oil-based graphite lubricants, with the average thickness error remaining below 1%. This outcome highlights the effective performance of both lubricant types in achieving the required dimensional specifications. As shown in Figure 5(b), which compares the measured dimensions to ball joint specifications, Section A demonstrates that the water-based graphite lubricant achieved a mean thickness closer to the specification (43.03 mm) than the oil-based graphite (42.86 mm), resulting in a notably lower error of 0.07% versus 0.32%. However, Section B indicates superior accuracy for the oil-based graphite lubricant, which yielded a smaller error of 0.67% compared to a significant 3.33% for the water-based graphite. In Section C, the oil-based lubricant maintained a perfect dimensional match, while the water-based graphite showed a slight deviation of 0.31%. Similarly, in Section D, oil-based graphite again demonstrated greater precision, with an error of only 0.06%, compared to 0.26% for the water-based variant. Overall, the oil-based graphite lubricant resulted in a lower average error of 0.26%, compared to 0.99% for the water-based graphite. These results indicate that while both lubricants are effective, oil-based graphite provides enhanced dimensional accuracy, as further detailed in Table 4.

The improved dimensional accuracy associated with oil-based graphite lubricants can be attributed to their superior lubrication stability and thermal insulation characteristics under hot forging conditions. Oil-based carriers form more consistent and durable lubricant films at the die-workpiece interface, effectively reducing interfacial friction and limiting material sticking. This promotes smoother metal flow and more controlled deformation, leading to enhanced shape precision. Furthermore, oil-based lubricants generally possess lower thermal conductivity than water-based types, which helps to maintain a stable temperature distribution throughout the forming process. Altan [7] emphasized that graphite in oil-based carriers exhibits better filmforming capabilities and thermal resistance at elevated temperatures, which directly supports improved dimensional control. Similar findings by Behrens et al. [5] and Barrau et al. [8] underline the importance of friction reduction and thermal management in achieving consistent geometry and minimizing die wear. Zhu et al. [10] further demonstrated, through FEM validation, the sensitivity of final part geometry to frictional conditions in hot forging. These tribological and thermal effects collectively explain the significantly lower dimensional error observed with oil-based lubricants (0.26%) in comparison to waterbased lubricants (0.99%) in this study.

To further understand the influence of the forging process on the quality of the final product, it is essential to examine not only the dimensional accuracy but also the internal structure of the material. During the forging process, material flow plays a critical role in determining the mechanical properties of the forged component. The distribution of flow lines, which are aligned with the material's elongation direction, significantly impacts the anisotropy of these properties [18]. If these flow lines are well-organized and aligned parallel to the working surface, the forged part will exhibit favorable mechanical characteristics. Conversely, disordered or misaligned flow lines can lead to mechanical weaknesses [5].

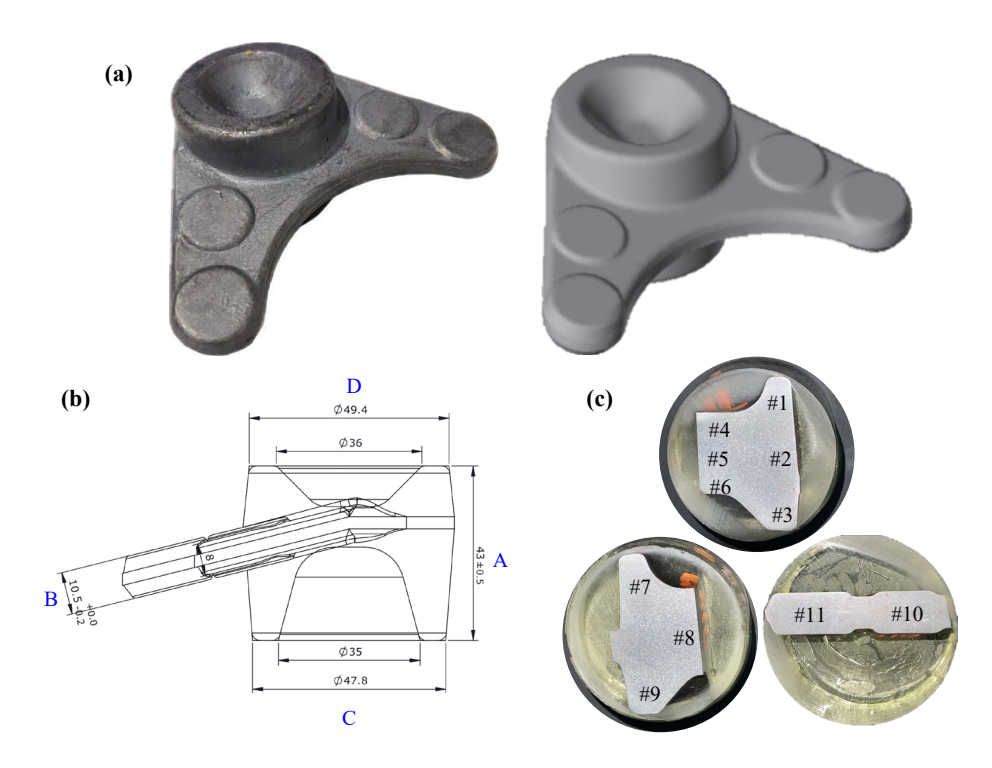


**Figure 5**. (a) Comparison of the final shapes of the ball joint between simulation results and the actual product; (b) Specifications of the ball joint dimensions; (c) Cross-section of the mounted ball joint prepared for microstructural analysis, showing the marked study points.

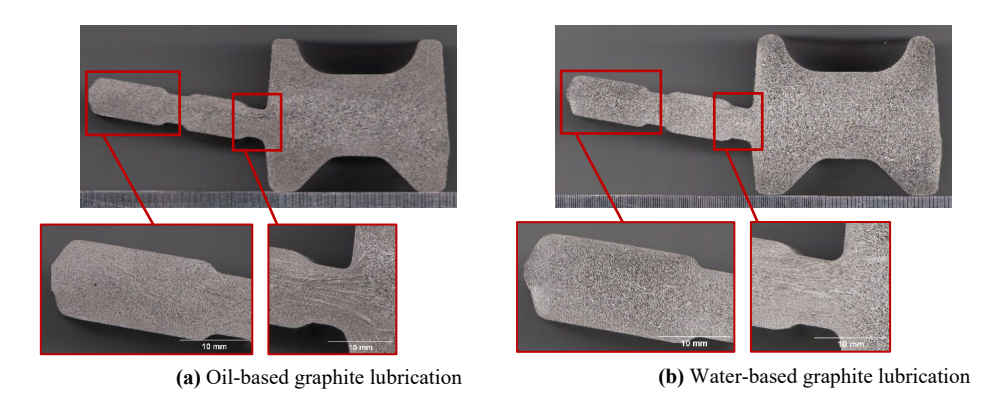


Figure 6 Optical microscopy (OM) images showing the distribution of flow lines observed in the cross-sections of forged parts under different lubrication conditions: (a) Oil-based graphite lubrication and (b) Water-based graphite lubrication.

In this study, Figure 6 displays optical microscopy (OM) images of distribution of the flow lines observed in cross sections. These findings highlight the critical role of material flow management in achieving both dimensional precision and strong mechanical performance during hot forging. The formation of flow lines is closely related to the stages of roughing and finishing in the forging process, where the billet is compressed radially, resulting in significant axial and radial metal flow. The analysis of the cross-section indicates that workpieces formed with oil-based graphite (Figure 6(a)) show a denser and more continuous distribution of metal flow lines compared to those formed with water-based graphite (Figure 6(b)), which exhibit fewer and less distinct flow lines. A well-defined metal flow path is indicative of uniform metal distribution, which is essential for enhancing the strength and ductility of the workpiece, particularly in applications that require high strength.

#### 3.3 Forming load

In the manufacturing of ball joints, lubrication significantly affects the forming load in both roughing and finishing processes, as illustrated in Figure 7(a), which compares predicted loads from finite element modeling (FEM) simulations with actual loads measured during forging. The actual forming loads were recorded directly from the digital display panel of the mechanical press, which indicates the peak force applied during each forging cycle; these values were manually read and documented for each lubrication condition. Under oil-based graphite lubrication, a forming load error of 16.23% was observed during roughing, with the FEM simulation predicting 4.67887 MN, compared to an actual average of 5.5852 MN. In the finishing stage, the error increased to 26.19%, with the predicted load at 4.68746 MN and the actual reaching 6.3503 MN. Conversely, water-based lubrication

exhibited greater prediction accuracy in the roughing stage, with only a 4.21% error (5.65762 MN FEM simulation vs. 5.9063 MN actual), although it consistently required higher forming loads in both stages. Specifically, during finishing, the error was 18.46%, with an actual load of 6.5478 MN. While water-based lubrication provided better agreement between FEM and experiment in the roughing stage, oil-based lubrication proved more beneficial overall due to its lower forming loads, which contribute to reduced energy consumption and tool wear which making it a more efficient and cost-effective choice for hot forging operations. Minor discrepancies between simulation and experiment may be attributed to machine compliance, thermal losses, or frictional variations not fully captured by the model.

#### 3.4 Grain size

Figure 5(c) shows the cross-section of the mounted ball joint, prepared for microstructural analysis, with marked study points. A detailed comparison of grain sizes in hot-forged ball joints, using oil-based and water-based graphite lubricants, was performed across 11 study points. This comparison is illustrated in Figure 7(b), which displays a bar graph of the average grain sizes for both lubricants. Further insights are provided in Figure 8, which presents the optical microstructures observed at these 11 study points in the ball joint cross-section. The results revealed that the oil-based lubricant produced a finer average grain size of approximately 13.50 μm, while the waterbased lubricant yielded an average grain size of about 23.52 µm. The standard deviation for the oil-based lubricant was approximately 4.82 μm, indicating a higher variability compared to the water-based lubricant, which had a standard deviation of about 3.12 µm. The oilbased lubricant produced a 42.60% finer average grain size compared to the water-based lubricant. This suggests that, although the oil-based lubricant facilitates better deformation characteristics during forging, it may lead to inconsistent lubrication performance. The finer grain size obtained with the oil-based lubricant could enhance the mechanical properties of the forged components, such as strength and toughness, due to the Hall–Petch relationship. However, the observed variability in grain size should be considered for ensuring consistent production quality, warranting further investigation into the effects of lubrication on the forging process and resulting material properties.

The finer grain size observed with oil-based graphite lubrication can be attributed to its superior tribological and thermal characteristics during hot forging. Oil-based lubricants are more effective at reducing interfacial friction, which promotes smoother metal flow and greater plastic strain distribution in the deformation zone. This condition enhances the initiation and progression of dynamic recrystallization (DRX), leading to more refined grains. In addition, the lower thermal conductivity of oil-based lubricants helps retain heat at the dieworkpiece interface, maintaining a favorable temperature for DRX to occur more extensively These combined effects accelerate recrystallization while preventing excessive grain growth. Previous studies have reported that improved lubrication and reduced thermal gradients facilitate microstructural refinement and DRX kinetics in hot forging processes [5,7]. These effects collectively explain the significantly finer and more uniform microstructure observed under oil-based lubrication conditions in this study.

## 3.5 Die wear

To verify die wear by comparing the results from FEM simulations with experimental observations, the maximum effective stress values from the simulations were analyzed. Table 5 below presents the stress values for both the roughing and finishing processes using water-based and oil-based lubricants. The upper and lower dies were evaluated in each scenario:

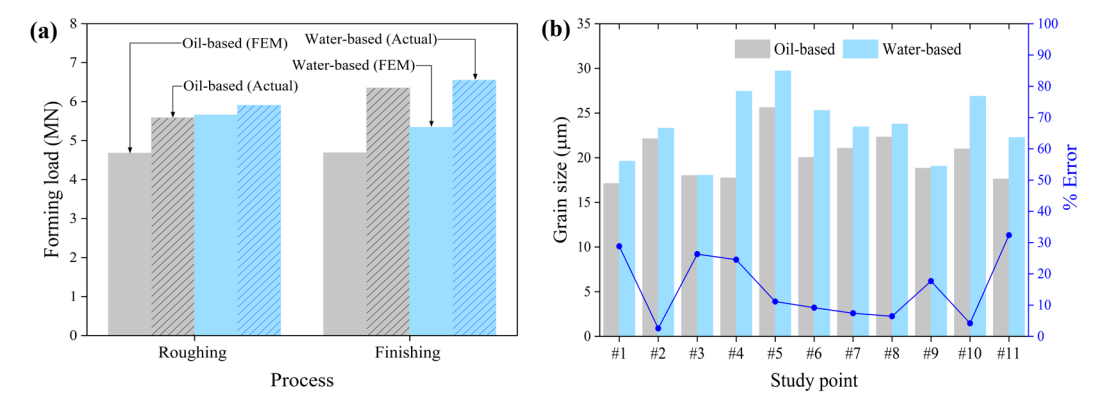


Figure 7. (a) Bar graph comparing the predicted and actual forming loads for oil-based and water-based lubricants used in ball joint manufacturing; (b) Bar graph comparing the grain size of hot-forged ball joints lubricated with oil-based and water-based graphite across 11 study points.

Table 5 Simulation results of maximum effective stress values in upper and lower dies for roughing and finishing processes.

Process	Lubricant	Upper die	Lower die	
		[MPa]	[MPa]	
Roughing	Water-based	1145.99	951.916	,
	Oil-based	617.435	686.326	
Finishing	Water-based	1352.28	1171.16	,
	Oil-based	1112.57	1086.86	

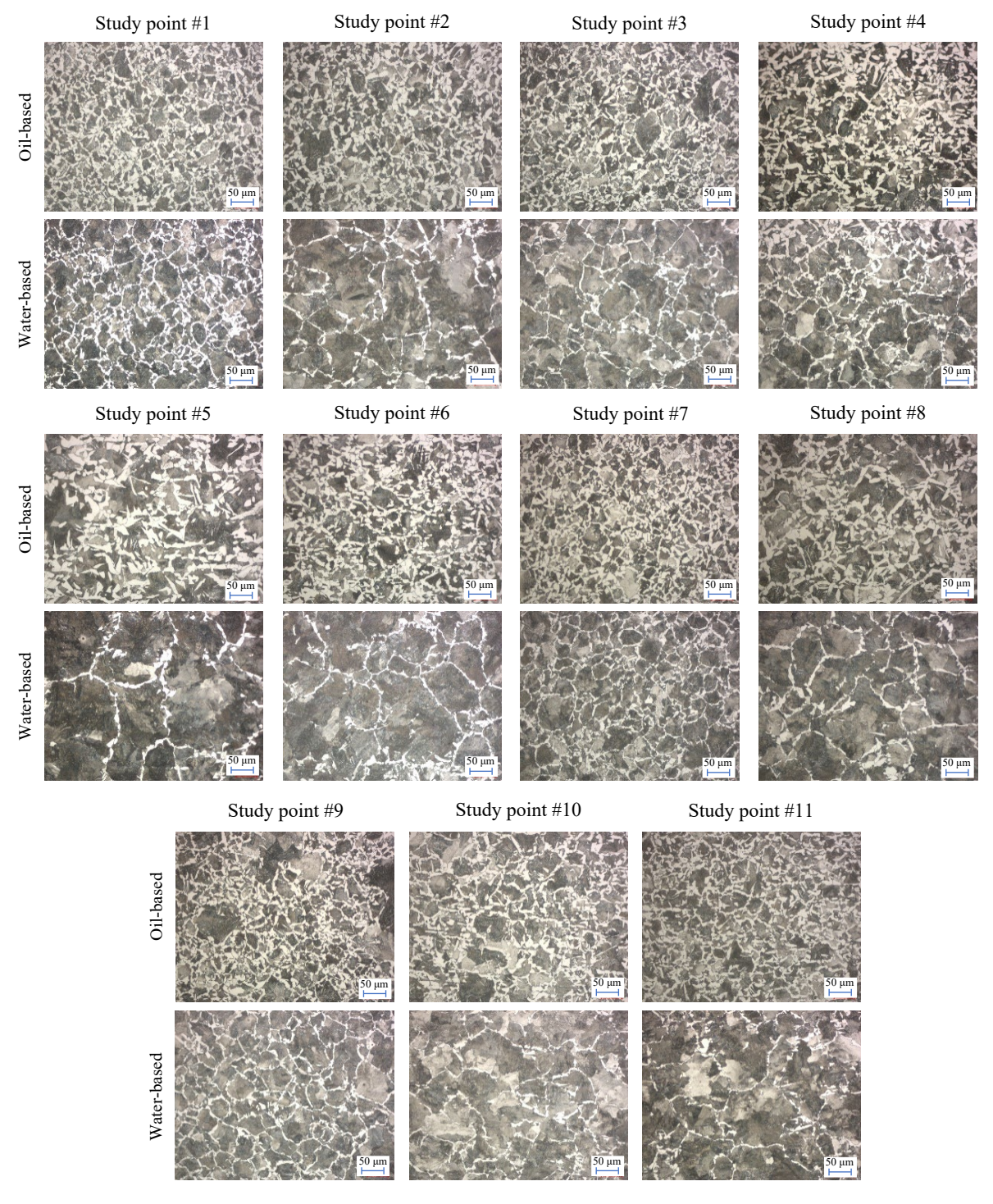


Figure 8. Optical microstructures at the 11-study point in the ball joint cross-section

The FEM simulation results reveal a clear distinction between the two types of lubricants. The water-based lubricant consistently produces significantly higher stress levels on both the upper and lower dies compared to the oil-based lubricant, in both the roughing and finishing processes. For instance, during roughing, the water-based lubricant generates a maximum effective stress of 1145.99 MPa on the upper die and 951.916 MPa on the lower die—almost double the stress levels recorded for the oil-based lubricant, which were 617.435 MPa and 686.326 MPa for the upper and lower dies, respectively. Similarly, in the finishing process, the water-based lubricant leads to higher stress,

with values reaching 1352.28 MPa and 1171.16 MPa for the upper and lower dies, respectively, compared to the oil-based lubricant's lower stress values of 1112.57 MPa and 1086.86 MPa. These findings suggest that the water-based lubricant, likely due to its lower lubrication efficiency, increases friction and contact pressure, which can contribute to faster die wear. In contrast, the oil-based lubricant, by generating lower stress levels, offers better lubrication performance, resulting in reduced wear and potentially extending the die's lifespan. This makes the oil-based lubricant more advantageous, particularly in the finishing process where precision and die longevity are crucial.

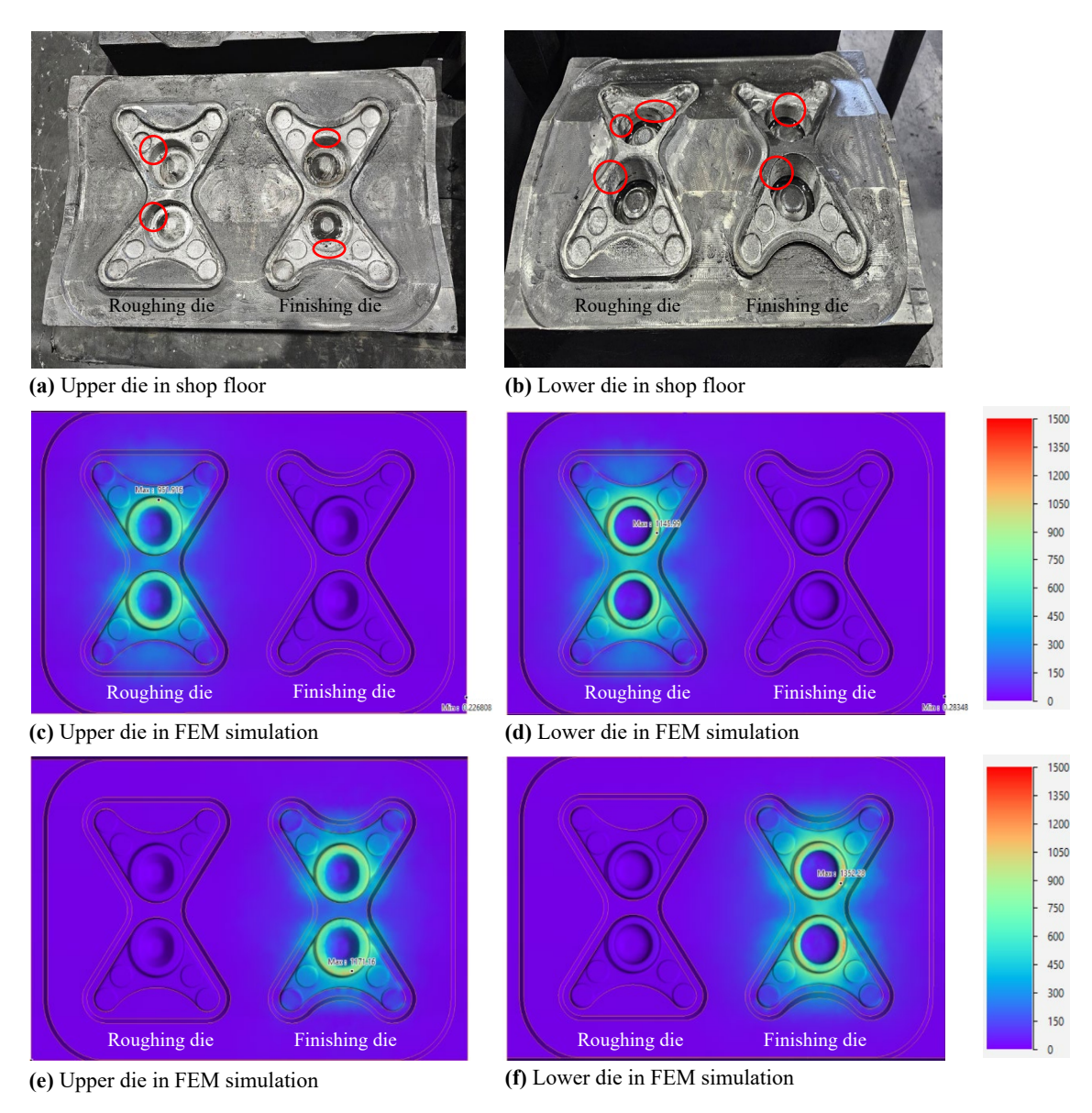


Figure 9. Comparison of die wear in real and simulated conditions: (a)—(b) Wear on upper and lower dies observed in the shop floor; (c)—(d) FEM simulation of wear on upper and lower dies at roughing process; and (e)–(f) Simulated wear on dies at finishing process.

The wear patterns observed on the shop floor using a water-based graphite lubricant further validate the simulation results, as shown in Figure 9. Although the image resolution limits the visibility of fine wear details, the general patterns visible in both the roughing and finishing stages qualitatively correspond with the higher stress regions predicted by FEM simulations. While the agreement is qualitative, it provides meaningful insight into the relationship between stress distribution and die surface wear. The upper die, particularly in the finishing stage, exhibited the most severe wear patterns, which corresponded to the highest stress levels in the simulations. In contrast, the lower die showed less pronounced wear patterns, consistent with the lower stress values. This qualitative agreement between the experimental observations and simulation results supports the validity of the FEM model in capturing the overall die wear behavior under varying lubrication conditions. Future studies will aim to enhance the clarity and precision of wear pattern validation by employing higher-magnification imaging or surface profilometry, allowing for more detailed comparisons between experimental and simulated wear distributions.

### 4. Conclusion

This research evaluated the influence of water-based and oil-based graphite lubricants on the hot forging performance of AISI 1045 medium carbon steel ball joints through FEM simulation, experimental trials, and microstructural characterization. Key findings are summarized as follows:

Modeling the Constitutive equation: A flow stress model was developed using hot compression test data, incorporating temperature and strain rate dependence to simulate material behavior accurately. The model was implemented into FEM to predict forming loads and flow characteristics under industrial conditions.

Dimensional Accuracy: Forged products under oil-based lubrication achieved higher dimensional precision, with an average error of only 0.26% compared to 0.99% for water-based lubrication.

Lubricant performance: Oil-based graphite lubricant significantly reduced forming loads and die stress compared to water-based graphite, with a 16.23% to 26.19% reduction in forming load and up to 46%

lower maximum die stress. This indicates better lubrication efficiency and reduced tool wear potential.

Microstructure refinement: The oil-based lubricant promoted finer grain structures, with an average grain size of 13.50  $\mu$ m, 42.6% finer than the 23.52  $\mu$ m observed with water-based lubricant. This was attributed to enhanced dynamic recrystallization due to lower interfacial friction and better thermal insulation.

Die Wear: FEM simulations of effective stress distribution qualitatively aligned with observed die wear patterns, supporting the model's reliability. The wear zones on the upper die during finishing matched regions of predicted high stress.

Overall, this work demonstrates that combining FEM simulation with experimental validation enables a comprehensive evaluation of process parameters in hot forging. The findings support the use of oil-based graphite lubricant to improve forging efficiency, dimensional control, and microstructural quality in automotive component manufacturing.

## Acknowledgement

The authors gratefully acknowledge the financial support provided by the Petchra Pra Jom Klao Master's Degree Research Scholarship from King Mongkut's University of Technology Thonburi, which made this research possible. Sincere appreciation is also extended to S.B.-CERA Co., Ltd. for generously sharing their technical expertise and providing invaluable assistance with the industrial components.

#### References

- [1] S. Debin, and Y. Lin, "5.14 Hot Forging," in Comprehensive Materials Processing, S. Hashmi, G. F. Batalha, C. J. Van Tyne, and B. Yilbas, Eds. Oxford, U.K.: Elsevier, 2014, pp. 275–289.
- [2] E. Tempelman, H. Shercliff, and B. N. van Eyben, "Ch. 6 Forging of Metals," in Manufacturing and Design, E. Tempelman,
  H. Shercliff, and B. N. van Eyben, Eds. Boston, MA, USA: Butterworth-Heinemann, 2014, pp. 85–103.
- [3] C. Caminaga, F. O. Neves, F. C. Gentile, and S. T. Button, "Study of alternative lubricants to the cold extrusion of steel shafts," *Journal of Materials Processing Technology*, vol. 182, no. 1, pp. 432–439, 2007.
- [4] N. Karunathilaka, N. Tada, T. Uemori, R. Hanamitsu, M. Fujii, Y. Omiya, and M. Kawano, "Effect of lubrication and forging load on surface roughness, residual stress, and deformation of cold forging tools," *Metals*, vol. 9, no. 7, p. 783, 2019.
- [5] B.-A. Behrens, A. Bouguecha, I. Lüken, J. Mielke, and M. Bistron, "Tribology in hot forging," *Comprehensive Materials Processing*, vol. 5, pp. 211–234, 2014.
- [6] F. Luis Fernando, S. Bruno Caetano dos Santos, B. Gilmar Ferreira, and C. Rodrigo Santiago, "The role of friction on metal forming processes," *Tribology of Machine Elements - Fundamentals and Applications*, p. 101387, 2022.
- [7] T. Altan, and G. S. Gracious Ngaile, Eds., "Cold and Hot Forging: Fundamentals and Applications, Materials Park, OH, USA: ASM International, 2005, p. 341.

- [8] O. Barrau, C. Boher, R. Gras, and F. Rezai-Aria, "Analysis of the friction and wear behaviour of hot work tool steel for forging," *Wear*, vol. 255, no. 7, pp. 1444–1454, 2003.
- [9] E. Daouben, A. Dubois, M. Dubar, L. Dubar, R. Deltombe, N. G. Truong Dinh, and L. Lazzarotto, "Effects of lubricant and lubrication parameters on friction during hot steel forging," *Intternation Journal of Material Forming*, vol. 1, pp. 1223–1226, 2008.
- [10] Y. Zhu, W. Zeng, X. Ma, Q. Tai, Z. Li, and X. Li, "Determination of the friction factor of Ti-6Al-4V titanium alloy in hot forging by means of ring-compression test using FEM," *Tribology International*, vol. 44, no. 12, pp. 2074–2080, 2011.
- [11] K. Asai, and K. Kitamura, "Estimation of frictional property of lubricants for hot forging of steel using low-speed ring compression test," Procedia Engngineering, vol. 81, pp. 1970–1975, 2014.
- [12] K. Asai, K. Kitamura, N. Yukawa, and N. Hayashi, "Estimation of friction by using improved calibration curves of ring compression test for hot forging of steel," *Procedia Engngineering*, vol. 207, pp. 2280–2285, 2017.
- [13] I. Serebriakov, E. S. Puchi-Cabrera, L. Dubar, P. Moreau, D. Meresse, and J. G. La Barbera-Sosa, "Friction analysis during deformation of steels under hot-working conditions," *Tribology International*, vol. 158, p. 106928, 2021.
- [14] F. Martín, M. J. Martín, L. Sevilla, and M. A. Sebastián, "The ring compression test: Analysis of dimensions and canonical geometry," *Procedia Engngineering*, vol. 132, pp. 326–333, 2015.
- [15] V. Mandic, "Friction studies utilizing the ring-compression test—Part I," *Tribology in Industry Journal*, vol. 25, 2003.
- [16] R. Poungprasert, N. Siripath, and S. Suranuntchai, "A comparative study of lubrication performance for BS 080M46 medium carbon steel using ring compression test and finite element simulation," *Key Engineering Materials*, vol. 973, pp. 37–44, 2024.
- [17] A. Srivastava, A. Srivastava, and A. Mishra, "Analysis of friction factor & coefficient of friction using ring compression test under various lubricants," *International Journal of Engineering Research and Technology*, vol. 9, no. 6, pp. 17–23, 2019.
- [18] R. Lima, and S. Button, "Application of the finite element method in cold forging processes," *Journal of the Brazilian Society of Mechanical Sciences and Engineering*, vol. 22, 2000.
- [19] D. Shahriari, A. Amiri, and M. H. Sadeghi, "Study on hot ring compression test of Nimonic 115 superalloy using experimental observations and 3D FEM simulation," *Journal of Materials Engineering and Performance*, vol. 19, no. 5, pp. 633–642, 2010.
- [20] M. Riaz, and N. Atiqah, "A study on the mechanical properties of S45C medium type carbon steel specimens under lathe machining and quenching conditions," *International Journal* of Engineering Research and Technology, vol. 3, pp. 121–130, 2014.
- [21] CHS-Asia Chemical Co., Ltd., Material safety data sheet RAMUDO L120, Samutprakarn, Thailand, 2017.

- [22] CHS-Asia Chemical Co., Ltd., Material safety data sheet RAMUDO MF161, Samutprakarn, Thailand, 2020.
- [23] CHS-Asia Chemical Co., Ltd., Product Data Sheet: RAMUDO L120, Bangkok, Thailand, 2018.
- [24] CHS-Asia Chemical Co., Ltd., Product Data Sheet: RAMUDO MF161, Bangkok, Thailand, 2017.
- [25] H. Yi, J. Ding, C. Ni, J. Dai, Y. Tang, X. Chen, K. Song, and X. Xia, "Hot compression deformation behavior and processing maps of Al–0.5Mg–0.4Si–0.1Cu alloy," *Journal of Materials Research and Technology*, vol. 19, pp. 4890–4904, 2022.
- [26] Y.-C. Lin, M.-S. Chen, and J. Zhang, "Modeling of flow stress of 42CrMo steel under hot compression," *Materials Science and Engineering A*, vol. 499, no. 1, pp. 88–92, 2009.
- [27] V. K. Kumar, and Neelam, "Modeling and multiple performance optimization of ultrasonic micro-hole machining of PCD using fuzzy logic and Taguchi quality loss function," *Advanced Materials Research*, vol. 1, no. 2, pp. 129–146, 2012.
- [28] N. Siripath, S. Suranuntchai, and S. Sucharitpwatskul, "Comparative study on material models for BS 080M46 medium carbon steel," *Engineering and Applied Science Research*, vol. 51, no. 1, p. 22, 2024.
- [29] C. Zener, and J. H. Hollomon, "Effect of strain rate upon plastic flow of steel," *Journal of Applied Physics*, vol. 15, no. 1, pp. 22–32, 1944.

- [30] Y. Xu, P. Birnbaum, S. Pilz, X. Zhuang, Z. Zhao, and V. Kräusel, "Investigation of constitutive relationship and dynamic recrystallization behavior of 22MnB5 during hot deformation," *Results in Physics*, vol. 14, p. 102426, 2019.
- [31] Z. Xiao, Q. Wang, Y. Huang, J. Hu, and M. Li, "Hot deformation characteristics and processing parameter optimization of Al-632Zn-210Mg alloy using constitutive equation and processing map," *Metals*, vol. 11, no. 2, p. 360, 2021.
- [32] T. R. Dandekar, R. K. Khatirkar, A. Gupta, N. Bibhanshu, A. Bhadauria, and S. Suwas, "Strain rate sensitivity behaviour of Fe–21Cr-1.5Ni–5Mn alloy and its constitutive modelling," *Materials Chemistry and Physics*, vol. 271, p. 124948, 2021.
- [33] Q. Liang, X. Liu, P. Li, P. Ding, and X. Zhang, "Development and application of high-temperature constitutive model of HNi55-7-4-2 alloy," *Metals*, vol. 10, no. 9, p. 1250, 2020.
- [34] X. Chen, N. Wang, X. Ma, and H. Zhou, "Hot deformation behaviour and Hansel-Spittel constitutive model of Cr<sub>5</sub> alloy for heavy backup roll," *International Journal of Computational Materials Science and Surface Engineering*, vol. 7, no. 3–4, pp. 205–217, 2018.
- [35] M. C. Kim, S. H. Chung, and M. S. Joun, "Optimal process design in hot forging in terms of grain flow quality," *International Journal of Automotive Technology*, vol. 20, no. 1, pp. 45–56, 2019.